Ivaniha, O.: Long-term analysis
of the Antarctic total ozone zonal asymmetry by MERRA-2
and CMIP6 data, Ukrainian Antarctic Journal, 1, 41—55, 2020.
doi:10.33275/1727-7485.1.2020.378

O. Ivaniha

Taras Shevchenko National University of Kyiv, Kyiv, 01601,Ukraine

Corresponding author: ivaoksi94@gmail.com

Long-term analysis of the Antarctic total ozone zonal asymmetry by MERRA-2 and CMIP6 data

Abstract. Objectives. To analyze ozone monthly mean data from the MERRA-2 reanalysis and CMIP6 model. To determine Antarctic ozone asymmetry climatology for austral spring months (September, October, November) over the 1980–2014 period. Methods. Processing and visualization of the MERRA-2, CMIP6 data on total ozone and ozone partial pressure, following analysis, interpretation, and comparison. Getting 2D (total ozone column) and 3D (ozone partial pressure) monthly mean ozone values for the zonal band (0°–90° S) at pressure levels (1000–0.1 hPa) for each month of the chosen period. Calculating climatology of the total ozone and ozone partial pressure. Comparison of model and reanalysis of results. Results. The amplitude of ozone zonal asymmetry was calculated to provide the monthly, latitudinal, longitudinal and altitudinal analysis. It is shown that the largest ozone zonal asymmetry is observed in spring, especially in October, with dominant wave-1 structure with zonal minimum over 0°–90° W, and maximum over 120°–180° E longitudinal sectors. The area with high ozone content is located at the 40°–80° S zonal band and gradually shifts to the south from September to November. The model underestimates amplitude of ozone zonal asymmetry, especially in October. Conclusions. Latitudinal mean maximums in zonal mean ozone distribution are observed over 62° S, in October over 66° S, and in November over 68° S for MERRA-2 and over 64° S, 65° S and 66° S respectively for CMIP6. The poleward shift of ozone latitude maximum continues until March with decreasing of ozone level, but in April, the shift reverses its direction to equatorward and ozone level starts to increase, however in the model this process is slower. In September the shift again becomes poleward. In the longitudinal distribution wave-1 pattern dominates with a shift of longitude ozone minimum. From September to October the shift is eastward, and from October to November westward by MERRA-2 data and only eastward by CMIP6 data. The highest difference in altitude ozone distribution is observed during October in the stratosphere between ozone zonal minimum and maximum points and reaches approximately 68% (44%) of the zonal average value at 65° S (65.4° S) by MERRA-2 (CMIP6) data. MERRA-2 profiles unlike CMIP6 one show higher location of altitudinal maximum over the zonal minimum and lower over the zonal maximum with the zonal mean in the middle. All three CMIP6 profiles have the same height of altitude maximum.

Keywords: ozone hole, planetary waves, climatology, zonal asymmetry, MERRA-2, CMIP6

1 Introduction

In the latest ozone depletion report, the World Meteorological Organization (WMO) (WMO, 2018) noted that although the ozone hole had diminished in size and depth since 2000, it was varying greatly from year to year depending on the state of the atmosphere. For example, the ozone hole was particularly large and long lasting in 2015, because of a cold and undisturbed polar stratospheric vortex and the Calbuco volcanic eruption (Ivy et al., 2017), which played a key role in that year's ozone depletion. Nonetheless,

in 2017 the Antarctic ozone hole was very small due to a warm and unusually disturbed polar vortex (Hirooka et al., 2018). In addition, recent observations show that the ozone hole in 2019 had the smallest size since it was discovered (Farman et al., 1985; Milinevsky et al., 2019).

Despite the positive trends of recent years, processes of ozone recovery are much slower than depletion development. Dhomse et al. (2018) conducted a deep analysis of chemical and climate models (20 models with 150 simulations have been considered) and showed that the time of ozone recovery would depend on the region. The fastest ozone recovery could be observed in the Northern hemisphere (2020–2044 years) and the slowest in the Antarctic ozone during spring (2055–2066). Global ozone values will return to the levels of 1980 in 2043–2055 (Dhomse et al., 2018).

Many observations (Grytsai et al., 2007; Ialongo et al., 2012; McPeters et al., 2015) and climate model simulations (Austin et al., 2010; Dennison at el., 2017) have shown that the ozone hole could play a dominant role in the forcing of stratospheric cooling trends in the Polar Regions. However, models with zonal mean total ozone column (TOC) could not be entirely realistic. According to Waugh et al. (2009), simulations with zonal mean ozone in spring–early summer describe a warmer stratosphere (and as a result, a weaker vortex) in comparison to a three-dimensional ozone field but there are only small differences in the polar stratospheric temperatures during periods with a weak or absent ozone hole. In addition, Antarctic temperature trends and troposphere circulation are underestimated when zonal mean ozone is described (Waugh et al., 2009). Gillett et al. (2009) also suggested that the inclusion of zonal asymmetry in ozone might be important for accurate simulation of future stratospheric temperature trends. They found a zonal mean temperature response to an ozone zonal asymmetry up to 4 K in the lower stratosphere. Simulations made by Rae et al. (2019) established that ozone zonal asymmetry affected the polar vortex and urged it to elongate and move to the region with the lower ozone level.

A large zonal asymmetry of springtime ozone over Antarctica is well investigated (Evtushevsky et al., 2008; Ialongo et al., 2012). Ozone zonal asymmetry (OZA) is observed when ozone hole moves relative to the pole because of planetary wave activity and ozone rich air accumulates in the Southeast sector 150° E–170° W (Ialongo et al., 2012) outside of the polar vortex. However the Antarctic ozone hole is not centered over the pole, but displaced towards the Atlantic sector at 40° E – 40° W (Ialongo et al., 2012), 0°–90° W (Grytsai et al., 2007), ~45° W (Dennison et al., 2017). Analysis of the Total Ozone Mapping Spectrometer (TOMS) data made by Grytsai et al. (2007) found the largest Antarctic OZA in September–November at about 60° S. Due to this work a mean sub-Antarctic zonal maximum is located in the sector 90°–180° E with total ozone level about 380 Dobson Units (DU) between 50°–60° S and minimum in the sector 0°–60° W with total ozone levels about 200 DU between 70°–80° S. Grytsai et al. (2007) also indicate that OZA was present in the years before the ozone hole as well and show the annual and lesser monthly (September–November) eastward shift of the zonal ozone minimum and stability of the zonal maximum (from the 1979 to 2005). Simulations made by Dennison et al. (2017) demonstrated that during ozone depletion the center longitude of ozone hole moved westerly, showing a shift up to 50°, and then in the 21st century ozone recovery forced an eastward trend.

Ialongo et al. (2012) showed that OZA during Antarctic winter–spring is formed under influence of the planetary waves with wave numbers from 1 to 3, which could explain ~95% of ozone variability. Nonetheless, the components with wave number higher than 2 are often comparable or below the root mean square of residuals. Quasi-stationary wave-1 dominates in this region and usually gives the main contribution to the OZA, while the wave-2 has a smaller amplitude and is mainly an eastward traveling wave. In the paper (Ialongo et al., 2012) based on OMI total ozone data it was shown that the wave amplitudes are larger in October and reach ~140 DU (~45% of zonal mean TOC) in wave-1 and only during November 2009 and 2010 the wave-2 component showed a large stationary component, comparable to wave-1. The predominance of the zonal wave-1 produces a wide longitudinal extension of the zonal maximum and minimum

(Grytsai et al., 2017). Grytsai et al. (2007) mentioned that the maximum amplitude of wave-2 was observed approximately 5° poleward in comparison to the wave-1 maximum (65° S) and the wave-2 to wave-1 ratio increased at polar latitudes.

In this paper, we provide an analysis of the ozone monthly mean data from the MERRA-2 reanalysis and CMIP6 model to determine Antarctic ozone asymmetry climatology for austral spring months (September–November) over the 1980–2014 period, and to compare model and reanalysis results. More information about MERRA-2 and CMIP6 can be found in the data and methods section and in the cited works therein.

2 Data and methods

MERRA-2 system description

The new version of the National Aeronautics and Space Administration (NASA) Modern-Era Retrospective analysis for Research and Applications version 2 (MERRA-2) reanalysis improves and expands the original version MERRA (Rienecker et al., 2011). The purpose of this reanalysis is to retrieve the multi-decadal meteorological data based on constant analysis and processing system (model and assimilation component).

In MERRA-2 reanalysis the fixed data analysis system (FDAS) is used (Punge, Giorgetta, 2007). MERRA-2 compared to MERRA includes improvements in atmospheric circulation model and can work with modern satellite data without loss of accuracy (Molod et al., 2015). Description of MERRA-2 and its initial assessment is presented in (Bosilovich et al., 2015). In (Gelaro et al., 2017) the overview of the MERRA-2 system and comparison of MERRA-2 with MERRA is presented.

MERRA-2 assimilates ozone and temperature profiles from the NASA Aura Microwave Limb Sounder (MLS) from August (for temperature) and October (for ozone) 2004 and until today (Bosilovich et al., 2015). Information about MLS ozone and temperature profiles can better represent vertical gradients of ozone in the model. Before October 2004, the MERRA-2 assimilated ozone field was based on measurements of the Solar Backscatter Ultraviolet Radiometer (SBUV) (Frith et al., 2014). Since October 1, 2004, data from SBUV have been replaced by TOC from ozone monitoring instrument (OMI) and stratospheric profiles MLS (Bosilovich et al., 2015).

In MERRA-2 reanalysis spatial and time variability of ozone are completely modelled with consideration of advection, chemistry, and satellite data analysis. Ozone chemistry in MERRA-2 is given as monthly average, two-dimensional (latitude and pressure) coefficients of ozone formation and decay.

MERRA-2 covers the period from 1980 to the present and has a spatial resolution of 0.5° by latitude and 0.625° by longitude with 42 vertical pressure levels — from the surface to 0.1 hPa, time resolution — from hours to months (NASA Global Modeling and Assimilation Office, 2015a–d). In this study, we used monthly averaged data from 1980 to 2018 (38 years).

Ozone partial pressure p_{O3} (mbar) was calculated from the ozone mass mixing ratio M_{O3} (g/g) using the following conversion:

$$p_{O3} = 0.602 \cdot 10^5 \cdot M_{O3} \cdot \textit{pressure}\ (\text{hPa}).$$

Climatology data were obtained from the monthly mean MERRA-2 data. Climatology gives 2D (total ozone column) and 3D (ozone partial pressure) mean ozone values for the zonal band (0°–90° S) at 42 pressure levels (1000–0.1 hPa) for each month of the 1980–2014 period.

MERRA-2 ozone data

MERRA-2 reanalysis is based on satellite data, but in some areas, it is difficult to measure ozone (during polar night or below dense clouds) by satellite. Temporal and spatial homogeneity in reanalysis is achieved by weighting and blending observations in a statistically optimal way. However, there is a big question of reanalysis data appropriateness and the occurrence of discontinuities, large bias, and unphysical patterns in them.

In MERRA-2 the total ozone error during SBUV period (by October 2004) is set to 6 DU. Afterwards (OMI period) the same error is equal 5 DU everywhere. Both numbers are within 2% of the globally

averaged total ozone and consistent with the level of agreement between independent measurements reported by McPeters et al. (2008) and Labow et al. (2013). McPeters et al. (2015) note that OMI exhibits a latitude-dependent low bias with respect to SBUV (from 0.5% between 60° S and 15° S to 2% near 60° N). SBUV partial column errors depend on the pressure and are estimated as 1.4 DU (15%) between 1000 and 631 hPa, 1.9 DU (11%–6%) in the lower-stratospheric layers, 100–63 hPa and 63–40 hPa, and 1 DU (25% to over 100%) in the upper-stratospheric and mesospheric layers (Wargan et al., 2017). MLS ozone profiles retrieval errors (i.e., root sum square of random-noise and smoothing errors) are dominated by smoothing errors due to coarse vertical resolution and generally vary from 0.8–6% in the middle stratosphere to 6–35% in the troposphere (Liu et al., 2010).

Wargan et al. (2017) have compared the MERRA-2 stratospheric ozone with the Nimbus-7 Total Ozone Mapping Spectrometer (TOMS), the Microwave Limb Sounder instrument on the Upper Atmosphere Research Satellite (UARS MLS), the Michelson Interferometer for Passive Atmospheric Sounding (MIPAS), the Stratospheric Aerosol and Gas Experiment II (SAGE II) and ozonesondes data. The main result of their work is that MERRA-2 agrees well with independent data and has a good representation of stratospheric ozone variability. The standard deviation of the differences between the reanalysis and satellite data is less than 5–10% everywhere except the regions with high variability and 10–20% for ozonesonde data respectively (Wargan et al., 2017). The integration of Aura MLS data has led to a better estimation of ozone in MERRA-2, however, it also produces a discontinuity that should be taken into account. For example, compared to MERRA, MERRA-2 is significantly more adequate at representing South Pole ozone from October 2004 onward, when Aura ozone data are assimilated. Separately, the standard deviation of the differences between MERRA-2 and the ozonesonde values drops from 12.5% between 1991 and 2004 to 5% between 2005 and 2014 (Gelaro et al., 2017). More detailed analysis of the ozone assimilation quality in MERRA-2 is given in (Wargan et al., 2017; Gelaro et al., 2017).

Discontinuities can be caused by satellite or instrument replacement, by assimilation with not homogenous basic parameters or by natural processes. Krizan et al. (2019) investigated discontinuities in the ozone data from MERRA-2 reanalysis in 1980–2017. They have detected the maximum amount of discontinues in 1993 and 2004. One of the possible explanations of 1993 maximum given in (Krizan et al., 2019) is the Pinatubo eruption in 1991. Another maximum in 2004 is obviously connected to the instrument transition (SBUV to EOS Aura) in 2004. Shangguan et al. (2019) have similarly identified discontinuities in ozone and temperature data in 2015 when version 2.2 of the MLS ozone data was replaced by version 4.2 and in 1998 when the Advanced TIROS (The Television Infrared Observation Satellite) Operational Vertical Sounder (ATOVS) was launched. According to (Krizan et al., 2019) below 4 hPa, the number of discontinuities is small (the stratosphere has fewer discontinuities than the troposphere), and they are generally insignificant. Nevertheless, the data above 4 hPa have significant discontinuities and unphysical patterns (see Fig. 1 in Krizan et al., 2019) which look unrealistic. However, the switch from SBUV to EOS Aura data in 2004 does not have a robust effect on ozone discontinuities existence below 4 hPa (Krizan et al., 2019).

Overall, the MERRA-2 ozone data are in good agreement with independent satellite and ozonesonde data. The errors do not exceed the standard deviation of the observed ozone therefore, the reanalysis is able to reproduce a natural ozone variability. Below 4 hPa, the number of discontinuities is small, and they are generally insignificant. In the troposphere, the number of discontinuities is greater than in the stratosphere, but they are generally insignificant. The switch from SBUV to EOS Aura data in 2004 does not have a robust influence on discontinuities occurrence below 4 hPa. Nonetheless, data above 4 hPa are not appropriate for accurate scientific research due to the huge amount of discontinues, unphysical patterns and high observation and assimilation errors.

CMIP6 Ozone

The Stratosphere–troposphere Processes And their Role in Climate/Atmospheric Chemistry and Climate

(SPARC/ACC) ozone data set was prepared for the Coupled Model Intercomparison Project phase 5 (CMIP5) by Cionni et al. (2011). They used climate models with interactive chemistry to characterize the evolution of tropospheric and zonal-mean stratospheric ozone data based on accessible observations. However, the Cionni et al. (2011) data had several weaknesses, including the underestimation of the Antarctic ozone hole and total ozone column in the southern polar latitudes during spring in the past and the restriction to a single greenhouse gas scenario for stratospheric ozone in the future. Ozone dataset for CMIP6 is designed by Chemistry Climate Model Initiative (CCMI) that consists of several models. CCMI models cover the lower and middle atmosphere in a fully interactive way (Morgenstern et al., 2017) and hence provide more reliable ozone fields in time and space. More details can be found in (Eyring et al., 2016).

Checa-Garcia et al. (2018) have investigated ozone radioactive forcing (RF) using CMIP6 and compared it with CMIP5. They have found that global total ozone RF is 80% larger estimated by CMIP6. Despite the significant changes with respect to CMIP5, the CMIP6 estimate is more relevant to the values provided by the Fifth Assessment Report (AR5) of the United Nations Intergovernmental Panel on Climate Change (IPCC) (provides an overview of the state of knowledge concerning the science of climate change) (Checa-Garcia et al., 2018). Checa-Garcia et al. (2018) have also compared the CMIP6 and Multisensor Reanalysis version 1 in the satellite era (MSL) ozone. They have compared MSL and CMIP6 trends (1980–2010) for the 90°–30° S, 90°–30° N zonal bands and globally averaged. The agreement is good, especially in the Southern Hemisphere. However, compared to reanalysis in CMIP6 Northern Hemisphere and global total ozone data fields have a negative bias.

In this work, historical monthly mean CMIP6 ozone data (Hegglin et al., 2016) (only volume mixing (vmr, mole/mole) is available) for 1980–2014 are used and compared to MERRA-2 ozone data. The CMIP6 ozone volume mixing data have 66 pressure levels (from 1034 to 0.0002 hPa), 96 latitude, and 144 longitude levels (approximately 1.89 by latitude and 2.5 by longitude grid). We used only Southern Hemisphere ozone up to 0.1 hPa.

Ozone partial pressure p_{O3} (mbar) was calculated from the ozone volume mass mixing ratio VM_{O3} (mole/mole) using the following conversion:

$$p_{O3} = VM_{O3} \cdot 10^5 \cdot pressure \text{ (hPa)}.$$

The column of ozone in DU between a level l_0 and an upper level l_n in a discrete vertical grid is estimated by the equation, taken from the CMIP6 Ozone forcing dataset: supporting information:

$$TOC = 10^6 \cdot \frac{RT_0}{g_0 p_0} \sum_{i=l_0}^{i=l_n} \frac{\chi_{O3}(i) + \chi_{O3}(i+1)}{2} \cdot (p(i) - p(i+1))$$

Where $R = 287.30$ JKg^{-1}K^{-1}, $T_0 = 273.15$ K, $p_0 = 101325$ Pa, $g_0 = 9.80665$ m/s^2, $\chi_{o3}(i) = VM_{O3}$ of O_3 at level i (mole/mole) and $p(i)$ = pressure at level i (hPa).

Climatology data were obtained from the monthly mean CMIP6 data similar to MERRA-2 data.

3 Results and discussion

Features of ozone latitudinal distribution in the Southern Hemisphere

In the upper stratosphere, ozone equilibrium distribution arises from the balance between its formation after the photolysis reaction of molecular oxygen and the destruction in catalytic cycles that include hydrogen, nitrogen oxides, chlorine, and bromine (Bozem et al., 2017). To maintain a high rate of ozone formation in equilibrium photochemical reactions (Chapman, 1929) it is necessary to have strong ultraviolet radiation with 320 nm wavelengths which is powerful only at equatorial latitudes. Thus, according to the observations most of the ozone is formed over the tropics, and then has to migrate to the poles. This migration (transport) of ozone occurs due to the Brewer-Dobson circulation (BDC) (Brewer, 1949; Dobson, 1956). The cause of this circulation is planetary waves activity which in extratropical latitudes disturb zonal mean airflow and cause a weak meridional drift (Butchart, 2014). These processes are stronger in the winter hemisphere.

In the seasonal longitude-latitude (or meridional) ozone distribution in the Southern Hemisphere (SH), there are two peculiarities — the hole over polar latitudes and the "collar" of high ozone level over sub-polar latitudes with clearly defined wave-1 structure (one maximum and minimum). Both the ozone hole and ozone "collar" are formed in August, destroyed in November, with maximums in September–October. Nonetheless, these two effects have different origins.

Ozone hole forms inside of the polar vortex. The vortex exists during polar winter when Antarctica is almost dark (May–October) and the temperature drops sharply, due to lack of sunlight. This leads to the increase of the polar westerly winds in the stratosphere because of a growing temperature gradient between the mid-latitudes and the pole. The polar westerly wind forms a transport barrier — a stratospheric vortex isolating the polar air from tropical and mid-latitudes (Waugh et al., 2017). Inside the vortex, the temperature can drop to –78 °C and even lower, which is sufficient for the formation of the polar stratospheric clouds (PSC). PSC are composed of ice crystals with traces of nitric and sulfuric acids (Varotsos, Tzanis, 2012), and serve as the primary source of ozone-depleting substances. The depth and area of the Antarctic ozone hole are mainly governed by the number of stratospheric clouds, chlorine and bromine concentration in the stratosphere, stratospheric temperature and amount of sunlight reaching the polar region (Dameris, 2010).

The rapid ozone depletion occurs when sunlight returns to Antarctica (in spring) and penetrates into the polar vortex. Ultraviolet radiation catalyzes reactions in the stratospheric clouds (see ex., Poole, McCormick, 1988), leading to the dissociation of ozone molecules, and as a result, formation of an ozone hole. Therefore the hole begins to grow in late winter (usually at the end of August) as the sun returns to Antarctica, reaches its maximum area and depth in middle September–early October and typically extends throughout Antarctica or even beyond. In November, when the temperature rises, polar vortex weakens. When it is destroyed, air from the lower latitudes can freely penetrate the polar region and the hole disappears (Varotsos, Tzanis, 2012).

Unlike the Polar Region where the ozone hole dominates, SH sub-polar and mid-latitudes (40°–80° S) demonstrate high TOC values — ozone "collar", but the ozone distribution is not uniform and shows significant asymmetry with a maximum in September and October (austral spring) (Grytsai et al., 2007; Ialongo et al., 2012). Ozone "collar" in subpolar latitudes forms because of BDC, which increases during winter when the temperature gradient between the tropics and pole is higher. At the end of winter–early spring ozone rich air reaches subpolar latitudes. In October, the ozone seasonal maximum is observed. In early summer, when BDC weakens, ozone starts to decompose photochemically (Schanz et al., 2014; Christiansen et al., 2017), reaching the lowest level in autumn. Ozone "collar" region has a horseshoe-like shape and is not static every year both spatially (oscillates around a mean minimum and maximum) and in TOC levels. Longitudinal ozone maximum of the "collar" is observed over the Indian Ocean south of Australia and its minimum — over the Atlantic Ocean and southern South America (Ialongo et al., 2012).

The amplitude of the ozone zonal asymmetry

Climatology study was done for MERRA-2 reanalysis and CMIP6 historical ozone data for the 1980–2014 period. To retrieve the amplitude of the ozone zonal asymmetry (OZA), the difference between the maximum and minimum TOC values in longitudinal distribution (TOC_{max}–TOC_{min}) was calculated. These values were used for the seasonal and latitudinal climatology over polar and subpolar SH regions. Altitudinal and longitudinal climatology study was done along 65° S for MERRA-2 and along 65.4 °S for CMIP6 datasets. Vertical error bars and shadowed areas shown in the plots reflect the standard deviation from the climatology (further SDFC). In SH these deviations did not exceed 55 DU in TOC data and 4 mPa in ozone partial pressure data for both reanalysis and model data. They were highest over the polar region in spring.

Comparison between MERRA-2 and CMIP6 data was done using relative percentage difference:

$$\frac{\text{data}_{\text{merra2}} - \text{data}_{\text{cmip6}}}{\text{data}_{\text{merra2}}} \cdot 100\%.$$

ISSN 1727-7485. Ukrainian Antarctic Journal, 1, 2020, doi:10.33275/1727-7485.1.2020.378

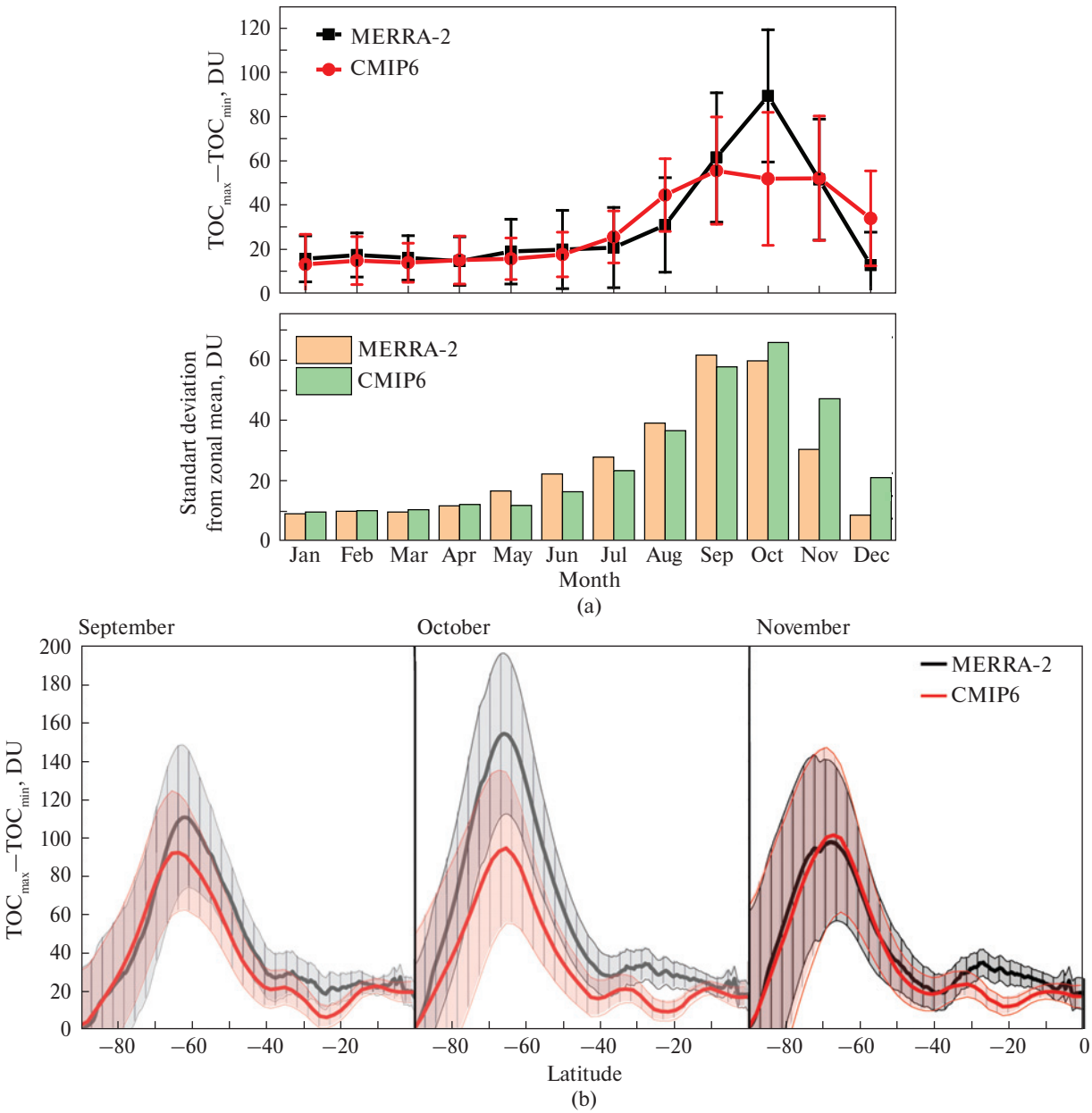

Figure 1. (a) Monthly mean ozone zonal asymmetry amplitude (upper plot, black MERRA-2 and red CMIP6 data) averaged by latitude (40°–80° S for MERRA-2 and 40.7°–80.5° S for CMIP6) along with standard deviation from latitudinal mean (color bars on the lower plot) and (b) latitudinal distribution of the ozone zonal asymmetry amplitude in September–November (shadowed areas represent the standard deviation from the climatology); monthly mean MERRA-2 and CMIP6 ozone data averaged over the 1980–2014 period climatology

Seasonal changes in the ozone distribution and, as a result, in OZA amplitude in mid-latitudes (linear relationship: higher TOC level–larger asymmetry), mainly are the result of dynamical processes such as the BDC, and the strength and position of the polar vortex. The climatological monthly mean amplitude of the zonal asymmetry averaged by latitude is shown in Fig. 1a (top plot). The data were averaged over the

40°–80° S latitudinal ring for MERRA-2 reanalysis and 40.7°–80.5° S for CMIP6 historical ozone for the 1980–2014 period. Both for MERRA-2 and for CMIP6 the peak of OZA occurs in spring. In October OZA amplitude by MERRA-2 data has a sharp peak, but by CMIP6 data its value is even lower than in September and November and the spring maximum is smoothed. In comparison to MERRA-2, CMIP6 underestimates OZA amplitude in October by 42.1% and overestimates it in August by 43.7%, and in December by 166.6%. In other months, this difference does not exceed 23%. Latitude mean OZA amplitude by MERRA-2 (CMIP6) data equals 61.5 DU (55.5 DU), 89.4 DU (51.8 DU) and 51.5 DU (52.1 DU) in September, October and November respectively, and over 15–30 DU in other months. Standard deviation from latitude mean (latitudinal variations, shown as vertical bars in Fig. 1a, lower plot) is comparable with longitudinal variation (but lower approximately by 20 DU) and peaks in spring. MERRA-2 latitudinal deviation (peak in September) is higher than CMIP6 one (peak in October) by 5 DU till September, then CMIP6 values become higher by 5–15 DU. SDFC (shown as error bars) are approximately 30 DU in spring and 10 DU in other months and have similar behavior — they are overestimated in summer and early autumn in CMIP6 compared to MERRA-2.

The OZA amplitude latitudinal variations are presented in Fig. 1b. The climatology over the 1980–2014 period was used. The area with high TOC level (ozone "collar") and as a result, high amplitude of the ozone zonal asymmetry in spring covers latitudinal ring of 40°–75° S. The equatorial edge (upper) of the ozone "collar" is defined as the region where the amplitude of the ozone zonal asymmetry begins to rise rapidly and the polar edge (lower) — by the polar vortex border. The maximum ozone asymmetry is observed at the ozone "collar" central latitude, which has the highest TOC level. This is a result of the linear relationship between TOC level and OZA amplitude. In September this latitude is around 62° S, in October — 66° S, and in November — 68° S for MERRA-2 and around 64° S, 65° S and 66° S respectively for CMIP6. Therefore, there is continuous poleward shift of the ozone "collar" central latitude from September to November, but in the model, this process is less pronounced in spring. Nevertheless, by monthly mean climatological meridional TOC distribution (not shown) this shift continues until March. In April the shift reverses to equatorward, but in September becomes poleward again and the cycle repeats. Such behaviour of TOC latitudinal distribution illustrates the interaction between the BDC and the polar vortex and their impact on the ozone distribution in mid- and subpolar latitudes. CMIP6 underestimates OZA amplitude in September up to 20% and in October up to 39% (CMIP6 October profile is very similar to September one), but November profile is very similar to MERRA-2 one. SDFC in September is from 5 to 42 DU by MERRA-2 data and is higher in sub-polar latitudes. In the model this value is lower by 1–10 DU everywhere. In October the SDFC values are very similar except for the polar vortex region, where CMIP6 shows values higher on 10–12 DU. In November SDFC values are the highest compared to other months — 2–55 DU with a peak over the polar region (similarly for both the model and reanalysis).

TOC level increases gradually when the intensity of the BDC grows in the SH (mid-autumn). It reaches maximum in spring. The BDC maximum is observed in the winter hemisphere, but ozone rich air arrives in subpolar latitudes with delay. That is why ozone maximum occurs there in spring. The position of the enhanced ozone "collar" relative to the pole is regulated by the polar vortex, which begins to form in the austral autumn and becomes the most powerful at the end of winter with a peak in August. When the polar vortex strengthens, ozone rich air shifts toward the equator (from April to September) because the vortex blocks the entrance to the polar latitudes. However, when the polar vortex weakens (from September to April) ozone rich air shifts to the pole, and in December when the vortex completely breaks down, it penetrates into the polar latitudes. This cycle is illustrated in the following papers (Waugh et al., 2017; Zhang et al., 2017). Underestimated OZA amplitude in CMIP6 and a slower shift to the pole peak latitude of ozone "collar" could indicate an unrealistic representation of the polar vortex and slower meridional transport in the model.

ISSN 1727-7485. Ukrainian Antarctic Journal, 1, 2020, doi:10.33275/1727-7485.1.2020.378

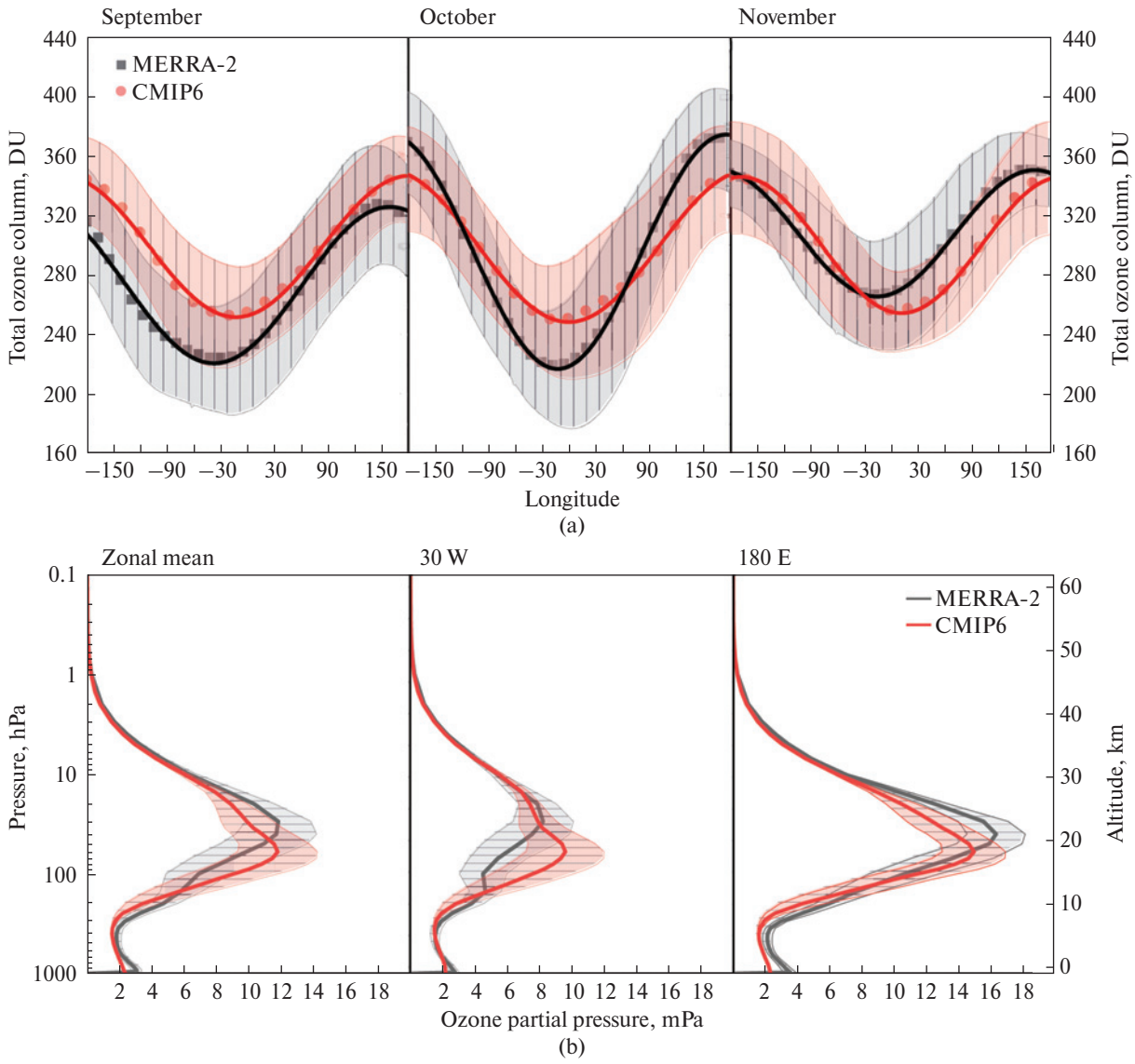

Figure 2. (a) Longitudinal distribution of the TOC in September–November over 65° S (points, partial) with sin fit (lines); (b) October zonal mean, over 30° W (zonal minimum) and 160° E (zonal maximum) altitude profiles of ozone partial pressure over 65° S. Monthly mean MERRA-2 and CMIP6 ozone data averaged over the 1980–2014 period climatology

The OZA amplitude longitudinal variations are shown in Fig. 2a. The climatology over the 1980–2014 period was used. Close latitude to ozone "collar" center (65° S for MERRA-2 and 65.4° S for CMIP6) and spring was chosen for analysis. As one can see in this figure, the quasi-stationary wave-1 dominates in TOC zonal distribution. Planetary waves with higher wavenumbers also exist but have noticeably smaller amplitude. In the ozone distribution, the longitudinal shift of the ozone zonal minimum (maximum) is observed for both model and reanalysis. The longitudinal shift of the zonal minimum is investigated using wave-1 amplitude (Fourier decomposition, first order, shown as a line in Fig. 2a). Wave-1 amplitudes for MERRA-2 (CMIP6) equal 52 DU (47 DU) for September, 79 DU (48 DU) for October, and 42 DU

(46 DU) for November. The positions of wave-1 zonal minimums are 32.6° W (12.9° W), 12.8° W (0° E), and 16.8° W (11.1° E) respectively. In MERRA-2 data an eastward shift of ozone zonal maximum is observed from September to October and a westward — from October to November. However, the ozone zonal minimum in CMIP6 only shifts eastward from September to November. In addition, CMIP6 data compared to MERRA-2 show a more eastward position of the ozone zonal minimum and wave-1 amplitude smaller by 39% in October. SDFC is higher for MERRA-2 near the zonal maximum in September and zonal minimum in November. Residuals from sinus approximations do not exceed 15 DU in September and 7 DU in October and November.

In the subpolar SH latitudes, a source of the stationary waves may be related to the planetary waves generated by the South America and Antarctica geography and thermal (ice/ocean) contrasts (Turner et al., 2017), as well as transitional tropospheric planetary waves associated with asymmetries in upper-tropospheric jet (Inatsu, Hoskins, 2004). By (Moustaoui et al., 2003), the stratospheric wave-1 perturbs the isentropic surfaces in such a way that ozone fields closely imitate the observed pattern in the stratospheric geopotential height (GPH) field. Moustaoui et al. (2003) note that ozone poor air from the polar vortex mixes with mid-latitudes air in areas where the potential vorticity is lower due to planetary waves dissipation and the position of TOC zonal minimum in the longitudinal distribution over the southwest Atlantic and South America determined by the higher level of planetary wave dissipation within this area. Nonrealistic representation of the ozone zonal minimum position in CMIP6 could be connected as well with nonrealistic representation of the polar vortex and planetary wave breaking. This is clearly seen in October when the polar vortex is most powerful and planetary waves are more active but CMIP-6 data show the highest difference with the reanalysis.

The OZA altitude variations are shown in Fig. 2b. The October profile climatology for the 1980–2014 period was used. The highest difference in ozone partial pressure is observed in the stratosphere around 200–10 hPa (10–30 km) for both model and reanalysis. Altitude ozone profiles near the zonal minimum and maximum are significantly different. The zonal mean, as expected, is close to average between zonal maximum and minimum. The differences are seen not only by the value but also by altitude where the maximum ozone partial pressure is observed. Thus, the altitude maximums of ozone partial pressure in October for MERRA-2 (CMIP6) are located at 30 hPa (65 hPa) for 30° W, at 40 hPa (65 hPa) for 180° E and at 35 hPa (65 hPa) for zonal-mean profiles. As can be seen from these numbers and Fig. 2b the CMIP6 ozone vertical profiles have the same altitude maximum for the zonal minimum and maximum and consequently for all latitudes because zonal mean profile has the same altitude maximum as well. MERRA-2 profiles unlike CMIP6 show higher position of altitude maximum over the zonal minimum and lower over zonal maximum with the zonal mean in the middle. Additionally, all MERRA-2 profiles have higher altitude maximums, but if one estimates ozone tropopause as a level with a sharp change of ozone partial pressure CMIP6 ozone tropopause will be always higher.

Evtushevsky et al. (2008) reported anticorrelation between TOC and tropopause height. The TOC values are related to the tropopause height, which in turn is influenced by the temperature of the lower stratosphere over Antarctica. In this connection, the tropopause elevates as the stratosphere cools. Decreases in TOC are associated with lower tropopause pressure (and the higher tropopause), and vice versa. Higher ozone tropopause in CMIP6 could indicate colder lower stratosphere in CMIP6 compared to MERRA-2.

The differences in the ozone partial pressure between the altitude maximum over 30° W and 180° E altitude profiles reach 8 mPa for MERRA-2 and 5.2 mPa for CMIP6, which is about 68% (44%) of the altitude maximum of the zonal mean profile. Despite the difference in ozone altitude maximum between CMIP6 and MERRA-2 (CMIP6 overestimates ozone altitude maximum over the zonal minimum and underestimates it over the zonal maximum) for zonal minimum and maximum profiles, zonal mean profiles have almost identical altitude maximum value (but

different position) over zonal mean. Deviations from zonal mean are higher for MERRA-2 — maximal value 3.5 mPa at 50 hPa pressure level (for CMIP6 this value is 2 mPa at 65 hPa pressure level). Maximal SDFC are observed 15–20 hPa lower than maximum altitude and are around 2.5–2.7 mPa for both model and reanalysis (model values are slightly higher).

4 Conclusions

Ozone climatology averaged over the 1980–2014 period has been analyzed. MERRA-2 reanalysis and CMIP6 model data were compared. The analysis deals with ozone data in the stratosphere over the polar and mid-latitudes of Southern Hemisphere with focus on austral spring months September–November. The spring season is chosen because during this period planetary waves and polar vortex are the most active.

In comparison to the Polar Region where during spring ozone hole dominates, subpolar and mid-latitudes (ozone "collar" at 40°–80° S) in the SH demonstrate high TOC level with a seasonal maximum in spring. However, its distribution is not uniform and has significant asymmetry which is strongest in October. Both ozone hole and ozone "collar" are formed in August and are destroyed in November with maximum reached in September–October. Nonetheless, in the model the ozone hole is more circular and centered over the pole, and ozone "collar" is shifted eastward compared to reanalysis. Ozone "collar" exhibits clear wave-1 structure with a zonal maximum over the Indian Ocean — the southern Australia area, and a minimum over South Atlantic Ocean and the south part of South America. The maximum ozone zonal asymmetry is observed in austral spring and peaks in October with the wave amplitude approximately 61.5 DU (55.5 DU), 89.4 DU (51.8 DU) and 51.5 DU (52.1 DU) in September, October and November respectively, and over 15–30 DU for MERRA-2 (CMIP6) data. In October OZA amplitude by MERRA-2 data has a sharp peak, but by CMIP6 data its value is even lower than in September and November and spring maximum is smoothed. In comparison to MERRA-2, CMIP6 underestimates OZA amplitude in October by 42.1% and overestimates it in August by 43.7%, and in December by 166.6%. In other months, this value does not exceed 23%. Standard deviation from longitude mean is comparable with longitude variation (lower approximately by 20 DU) and also peaks in spring. MERRA-2 latitude deviation (peak in September) is higher than CMIP6 one (peak in October) by 5 DU till September, than CMIP6 values become higher by 5–15 DU. Standard deviation from the climatological mean (approximately 30 DU in spring and 10 DU in other months) behaves similarly — it is overestimated in summer and early autumn in CMIP6 compared to MERRA-2.

The continuous poleward shift of the ozone "collar" central latitude from September to November is observed. In September this latitude is around 62° S, in October — 66° S, and in November — 68° S for MERRA-2 and 64° S, 65° S and 66° S respectively for CMIP6. The shift continues until March. In April it reverses to equatorward, and in September, again becomes poleward and the cycle repeats. Such behavior of TOC latitudinal distribution illustrates the interaction between the BDC and the polar vortex, and their impact on the ozone distribution in mid- and subpolar latitudes. Underestimation of OZA amplitude (in September up to 20% and in October up to 39%) in CMIP6 and a slower shift to the pole of the peak latitude of ozone "collar" could indicate unrealistic representation of the polar vortex and slower meridional transport in the model.

The longitudinal shift of the zonal minimum is investigated using wave-1 amplitude (Fourier decomposition, fist order). Wave-1 amplitudes for MERRA-2 (CMIP6) equal 52 DU (47 DU) for September, 79 DU (48 DU) for October and 42 DU (46 DU) for November and the position of wave-1 zonal minimum — 32.6° W (12.9° W), 12.8W (0° E), 16.8° W (11.1° E) respectively. In MERRA-2 data an eastward shift of ozone zonal maximum is observed from September to October, and a westward — from October to November. However, the ozone zonal minimum in CMIP6 is only shifted eastward from September to November. In addition, CMIP6 data compared to MERRA-2 show a more eastward position of the ozone zonal minimum and noticeably smaller amplitude of wave-1 in October by 39%.

The highest difference in ozone partial pressure is observed in the stratosphere around 200–10 hPa or 10–30 km. The differences in the ozone partial pressure between the altitude maximum over 30° W and 180° E altitude profiles reach 8 mPa for MERRA-2 and 5.2 mPa for CMIP6, which is about 68% (44%) of the altitude maximum of the zonal mean profile. Despite the difference in ozone altitude maximum between CMIP6 and MERRA-2 (CMIP6 overestimates ozone altitude maximum over the zonal minimum and underestimates it over the zonal maximum) for zonal minimum and maximum profiles, zonal mean profiles have almost identical altitude maximum value (but different positions) of zonal mean. MERRA-2 profiles, unlike CMIP6, show higher position of altitude maximum over the zonal minimum and lower over zonal maximum with the zonal mean in the middle. All three CMIP6 profiles have the same position of the altitude maximum.

Author contributions. The manuscript has been fully written by Ivaniha O. The author agrees with the published version of the manuscript.

Competing interests. The authors declare that they have no conflict of interest.

Acknowledgements. This work was supported in part by Taras Shevchenko National University of Kyiv projects 19BF051–08 and 20BF051-02, and PACT Project of SCAR Action group. The author thanks Gennadi Milinevsky, Asen Grytsai and Oleksandr Evtushevsky from Taras Shevchenko National University of Kyiv for valuable discussion and advices and the anonymous referee for the valuable comments and helpful suggestions that improved the manuscript. The author also thanks the NASA–GMAO for the MERRA-2 reanalysis data, IGAC/SPARC Chemistry-Climate Model Initiative for CMIP6 data, the Panoply netCDF, HDF and GRIB Data Viewer (https://www.giss.nasa.gov/tools/panoply/).

References

Austin, J., Struthers, H., Scinocca, J., Plummer, D.A., Akiyoshi, H., Baumgaertner, A.J.G., Bekki, S., Bodeker, G.E., Braesicke, P., Brühl, C., Yamashita, Y.: Chemistry-climate model simulations of spring Antarctic ozone, Journal of Geophysical Research, 115 (D3), D00M11, doi:10.1029/2009jd013577, 2010.

Bosilovich, M. G., Akella, S., Coy, L., Cullather, R., Draper, C., Gelaro, R., Kovach, R., Liu, Q., Molod, A., Norris, P., Suarez, M.: MERRA-2: Initial Evaluation of the Climate, Technical Report Series on Global Modeling and Data Assimilation, NASA/TM–2015–104606, 43, edited by: Koster, R.D., Goddard Space Flight Center, Greenbelt, Maryland, 139 pp., https://gmao.gsfc.nasa.gov/pubs/docs/Bosilovich803.pdf, 2015, last access: 23 February 2020.

Bozem, H., Butler, T.M., Lawrence, M.G., Harder, H., Martinez, M., Kubistin, D., Lelieveld, J., Fischer, H.: Chemical processes related to net ozone tendencies in the free troposphere, Atmospheric Chemistry and Physics, 17, 10565–10582, doi:10.5194/acp-17-10565-2017, 2017.

Brewer, A.W.: Evidence for a world circulation provided by the measurements of helium and water vapour distribution in the stratosphere, Quarterly Journal of the Royal Meteorological Society, 75 (326), 351–363, doi:10.1002/qj.49707532603, 1949.

Butchart, N.: The Brewer-Dobson circulation, Reviews of Geophysics, 52 (2), 157–184, doi:10.1002/2013rg000448, 2014.

Chapman, S.: A theory of upper atmospheric ozone, Memoirs of the Royal Meteorological Society, 3 (26), 103–125, 1929.

Christiansen, B., Jepsen, N., Kivi, R., Hansen, G., Larsen, N., Korsholm, U.S.: Trends and annual cycles in soundings of Arctic tropospheric ozone, Atmospheric Chemistry and Physics, 17, 9347–9364, doi:10.5194/acp-17-9347-2017, 2017.

Checa-Garcia, R., Hegglin, M. I., Kinnison, D., Plummer, D. A., Shine, K. P.: Historical tropospheric and stratospheric ozone radiative forcing using the CMIP6 database, Geophysical Research Letters, 45 (7), 3264–3273, doi:10.1002/2017GL076770, 2018.

Cionni, I., Eyring, V., Lamarque, J.F., Randel, W.J., Stevenson, D.S., Wu, F., Bodeker, G.E., Shepherd, T.G., Shindell, D.T., Waugh, D. W.: Ozone database in support of CMIP5 simulations: results and corresponding radiative forcing, Atmospheric Chemistry and Physics, 11 (21), 11267–11292, doi:10.5194/ acp-11-11267-2011, 2011.

Dameris, M.: Depletion of the ozone layer in the 21st century, Angewandte Chemie International Edition, 49 (3), 489–491, doi:10.1002/anie.200906334, 2010.

Dennison, F., McDonald, A., Morgenstern, O.: The evolution of zonally asymmetric austral ozone in a chemistry-climate model, Atmospheric Chemistry and Physics, 17, 14075–14084, doi:10.5194/acp-17-14075-2017, 2017.

Dhomse, S.S., Kinnison, D., Chipperfield, M.P., Salawitch, R.J., Cionni, I., Hegglin, M.I., Abraham, N.L., Akiyoshi, H., Archibald, A.T., Bednarz, E.M., Zeng, G.: Estimates of ozone return dates from Chemistry-Climate Model Initiative simulations, Atmospheric Chemistry and Physics, 18, 8409–8438, doi:10.5194/acp-18-8409-2018, 2018.

Dobson, G.M.B.: Origin and distribution of the polyatomic molecules in the atmosphere. Proceedings of the Royal

Society A, Mathematical, Physical and Engineering Sciences, 236 (1205), 187–193, doi:10.1098/rspa.1956.0127, 1956.

Evtushevsky, O.M., Grytsai, A.V., Klekociuk, A.R., Milinevsky, G.P.: Total ozone and tropopause zonal asymmetry during the Antarctic spring, Journal of Geophysical Research, 113 (D7), doi:10.1029/2008jd009881, 2008.

Eyring, V., Bony, S., Meehl, G.A., Senior, C.A., Stevens, B., Stouffer, R.J., Taylor, K.E.: Overview of the Coupled Model Intercomparison Project Phase 6 (CMIP6) experimental design and organization, Geoscientific Model Development, 9, 1937–1958, doi:10.5194/gmd-9-1937-2016, 2016.

Farman, J., Gardiner, B., Shanklin, J.: Large losses of total ozone in Antarctica reveal seasonal ClO_x/NO_x interaction, Nature, 315, 207–210, doi:10.1038/315207a0, 1985.

Frith, S.M., Kramarova, N.A., Stolarski, R.S., McPeters, R.D., Bhartia, P.K., Labow, G.J.: Recent changes in total column ozone based on the SBUV version 8.6 merged ozone data set, Journal of Geophysical Research: Atmospheres, 119 (16), 9735–9751, doi:10.1002/2014jd021889, 2014.

Gelaro, R., McCarty, W., Suárez, M.J., Todling, R., Molod, A., Takacs, L., Randles, C.A., Darmenov, A., Bosilovich, M.G., Reichle, R., Zhao, B.: The Modern-Era Retrospective Analysis for Research and Applications, Version 2 (MERRA-2), Journal of Climate, American Meteorological Society, 30 (14), 5419–5454, doi:10.1175/jcli-d-16-0758.1, 2017.

Gillett, N.P., Scinocca, J.F., Plummer, D.A., Reader, M.C.: Sensitivity of climate to dynamically-consistent zonal asymmetries in ozone, Geophysical Research Letters, 36 (10), doi:10.1029/2009gl037246, 2009.

Grytsai, A.V., Evtushevsky, O.M., Agapitov, O.V., Klekociuk, A.R., Milinevsky, G.P.: Structure and long-term change in the zonal asymmetry in Antarctic total ozone during spring, Annales Geophysicae, 25 (2), 361–374, doi:10.5194/angeo-25-361-2007, 2007.

Grytsai, A., Klekociuk, A., Milinevsky, G., Evtushevsky, O., Stone, K.: Evolution of the eastward shift in the quasistationary minimum of the Antarctic total ozone column, Atmospheric Chemistry and Physics, 17, 1741–1758, doi:10.5194/acp-17-1741-2017, 2017.

Hegglin, M.I., Kinnison, D., Lamarque, J.-F., Plummer, D.: CCMI ozone in support of CMIP6 — version 1.0, Earth System Grid Federation, doi:10.22033/ESGF/input4MIPs.1115, 2016.

Hirooka, T., Liu, G., Eguchi, N.: Small Antarctic Ozone Hole in 2012 and 2017 and the Relationship to Dynamical Fields, in: AGU Fall Meeting Abstracts, A51S-2541, 2018.

Ialongo, I., Sofieva, V., Kalakoski, N., Tamminen, J., Kyrölä, E.: Ozone zonal asymmetry and planetary wave characterization during Antarctic spring, Atmospheric Chemistry and Physics, 12, 2603–2614, doi:10.5194/acp-12-2603-2012, 2012.

Inatsu, M., Hoskins, B.J.: The zonal asymmetry of the Southern Hemisphere winter storm track, Journal of Climate, 17 (24), 4882–4892, doi:10.1175/JCLI-3232.1, 2004.

Ivy, D.J., Solomon, S., Kinnison, D., Mills, M.J., Schmidt, A., Neely III, R.R.: The influence of the Calbuco eruption on the 2015 Antarctic ozone hole in a fully coupled chemistry-climate model, Geophysical Research Letters, 44 (5), 2556–2561, doi:10.1002/2016GL071925, 2017.

Krizan, P., Kozubek, M., Lastovicka, J.: Discontinuities in the ozone concentration time series from MERRA 2 reanalysis, Atmosphere, 10 (12), 812, doi:10.3390/atmos10120812, 2019.

Labow, G. J., McPeters, R. D., Bhartia, P. K., Kramarova, N.: A comparison of 40 years of SBUV measurements of column ozone with data from the Dobson/Brewer network, Journal of Geophysical Research: Atmospheres, 118 (13), 7370–7378, doi:10.1002/jgrd.50503, 2013.

Liu, X., Bhartia, P. K., Chance, K., Froidevaux, L., Spurr, R.J.D., Kurosu, T.P.: Validation of Ozone Monitoring Instrument (OMI) ozone profiles and stratospheric ozone columns with Microwave Limb Sounder (MLS) measurements, Atmospheric Chemistry and Physics, 10 (5), 2539–2549, doi:10.5194/acp-10-2539-2010, 2010.

McPeters, R.D., Kroon, M., Labow, G., Brinksma, E., Balis, D., Petropavlovskikh, I., Veefkind, J.P., Bhartia, P.K., Levelt, P.F.: Validation of the Aura Ozone Monitoring Instrument total column ozone product, Geophysical Research Letters, 113 (D15), D15S14, doi:10.1029/2007JD008802, 2008.

McPeters, R.D., Frith, S., Labow, G.J.: OMI total column ozone: extending the long-term data record, Atmospheric Measurement Techniques, 8 (11), 4845–4850, doi:10.5194/amt-8-4845-2015, 2015.

Milinevsky, G., Evtushevsky, O., Klekociuk, A., Wang, Y., Grytsai, A., Shulga, V., Ivaniha, O.: Early indications of anomalous behavior in the 2019 spring ozone hole over Antarctica, E-print arXiv:1909.07574, https://arxiv.org/abs/1909.07574, 2019, last access: 17 March 2020.

Molod, A., Takacs, L., Suarez, M., Bacmeister, J.: Development of the GEOS-5 atmospheric general circulation model: evolution from MERRA to MERRA2, Geoscientific Model Development, 8, 1339–1356, doi:10.5194/gmd-8-1339-2015, 2015.

Morgenstern, O., Hegglin, M.I., Rozanov, E., O'Connor, F.M., Abraham, N.L., Akiyoshi, H., Archibald, A.T., Bekki, S., Butchart, N., Chipperfield, M.P., Zeng, G.: Review of the global models used within phase 1 of the Chemistry-Climate Model Initiative (CCMI), Geoscientific Model Development, 10, 639–671, doi:10.5194/gmd-10-639-2017, 2017.

Moustaoui, M., Teitelbaum, H., Valero, F.P.J.: Vertical displacements induced by quasi-stationary waves in the Southern Hemisphere stratosphere during spring, Monthly Weather Review, 131 (10), 2279–2289, doi:10.1175/1520-0493(2003)131 < 2279:VDIBQW>2.0.CO;2, 2003.

NASA Global Modeling and Assimilation Office, MERRA-2 inst3_3d_asm_Nv: 3d,3–Hourly, Instantaneous, Model–Level, Assimilation, Assimilated Meteorological Fields V5.12.4., doi:10.5067/WWQSXQ8IVFW8, 2015a.

NASA Global Modeling and Assimilation Office, MERRA-2 instM_3d_asm_Np: 3d, Monthly mean, Instantaneous, Pressure–Level, Assimilation, Assimilated Meteorological Fields V5.12.4. doi:10.5067/2E096JV59PK7, 2015b.

NASA Global Modeling and Assimilation Office, MERRA-2 tavgM_3d_odt_Np: 3d, Monthly mean, Time–Averaged, Pressure–Level, Assimilation, Ozone Tendencies V5.12.4. doi:10.5067/Z2KCWAV4GPD2, 2015c.

NASA Global Modeling and Assimilation Office, MERRA-2 tavgM_3d_trb_Np: 3d, Monthly mean, Time–Averaged, Pressure–Level, Assimilation, Turbulence Diagnostics V5.12.4. doi:10.5067/2YOIQB5C3ACN, 2015d.

Poole, L.R., McCormick, M.P.: Polar stratospheric clouds and the Antarctic ozone hole, Journal of Geophysical Research, 93 (D7), 8423–8430, doi:10.1029/JD093iD07p08423, 1988.

Punge, H.J., Giorgetta, M.A.: Differences between the QBO in the first and in the second half of the ERA-40 reanalysis, Atmospheric Chemistry and Physics, 7, 599–608, doi:10.5194/acp-7-599-2007,2007.

Rae, C.D., Keeble, R.J., Hitchcock, P., Pyle, J.A.: Prescribing zonally asymmetric ozone climatologies in climate models: performance compared to a chemistry-climate model, Journal of Advances in Modeling Earth Systems, 11 (4), 918–933, doi:10.1029/2018MS001478, 2019.

Rienecker, M.M., Suarez, M.J., Gelaro, R., Todling, R., Bacmeister, J., Liu, E., Bosilovich, M.G., Schubert, S.D., Takacs, L., Kim, G.-K., Woollen, J.: MERRA: NASA's modern-era retrospective analysis for research and applications, Journal of Climate, 24 (14), 3624–3648, doi:10.1175/JCLI-D-11-00015.1, 2011.

Schanz, A., Hocke, K., Kämpfer, N.: Daily ozone cycle in the stratosphere: global, regional and seasonal behaviour modelled with the whole atmosphere community climate model, Atmospheric Chemistry and Physics, 14 (14), 7645–7663, doi:10.5194/acp-14-7645-2014, 2014.

Shangguan, M., Wang, W., Jin, S.: Variability of temperature and ozone in the upper troposphere and lower stratosphere from multi-satellite observations and reanalysis data, Atmospheric Chemistry and Physics, 19 (10), 6659–6679, doi:10.5194/acp-19-6659-2019, 2019.

Turner, J., Hosking, J.S., Bracegirdle, T.J., Phillips, T., Marshall, G.J.: Variability and trends in the Southern Hemisphere high latitude, quasi-stationary planetary waves, International Journal of Climatology, 37 (5), 2325–2336, doi:10.1002/joc.4848, 2017.

Varotsos, C., Tzanis, C.: A new tool for the study of the ozone hole dynamics over Antarctica, Atmospheric Environment, 47, 428–434, doi:10.1016/j.atmosenv.2011.10.038, 2012.

Wargan, K., Labow, G., Frith, S., Pawson, S., Livesey, N., Partyka, G.: Evaluation of the Ozone Fields in NASA's MERRA-2 Reanalysis, Journal of Climate, American Meteorological Society, 30 (8), 2961–2988, doi:10.1175/JCLI-D-16-0699.1, 2017.

Waugh, D.W., Oman, L., Newman, P.A., Stolarski, R.S., Pawson, S., Nielsen, J.E., Perlwitz, J.: Effect of zonal asymmetries in stratospheric ozone on simulated Southern Hemisphere climate trends, Geophysical Research Letters, 36 (18), doi:10.1029/2009GL040419, 2009.

Waugh, D.W., Sobel, A.H., Polvani, L.M.: What is the polar vortex and how does it influence weather? Bulletin of the American Meteorological Society, 98, 37–44, doi:10.1175/BAMS-D-15-00212.1, 2017.

WMO. Executive Summary: Scientific Assessment of Ozone Depletion: 2018. Technical Report Report No. 58, 67 pp., Global Ozone Research and Monitoring Project, Geneva, Switzerland, 2018.

Zhang, Y., Li, J., Zhou, L.: The Relationship between Polar Vortex and Ozone Depletion in the Antarctic Stratosphere during the Period 1979–2016, Advances in Meteorology, 2017, 1–12, doi:10.1155/2017/3078079, 2017.

Received: 19 March 2020
Accepted: 19 May 2020

О. Іваніга

Київський національний університет імені Тараса Шевченка, м. Київ, 01601, Україна

Автор для кореспонденції: ivaoksi94@gmail.com

Аналіз довгострокової асиметрії в зональному розподілі озону над Антарктикою за даними MERRA-2 і CMIP6

Реферат. Мета. Проаналізувати середньомісячні дані загального вмісту та розподілу концентрації озону з реаналізу MERRA-2 та моделі CMIP6. Розрахувати кліматологію озону над Антарктикою протягом весняних місяців (вересень, жовтень, листопад) за 1980–2014 роки. Методи. Обробка і візуалізація загального вмісту і вертикальних профілів парційного тиску озону за даними MERRA-2 і CMIP6, подальший аналіз, інтерпретація та порівняння. Отримання 2D (загальний вміст озону) і 3D (парційний тиск озону) кліматологічно-середніх полів даних для зональної смуги (0°–90° пд.ш.) на рівнях тиску (1000–0.1 гПа) для кожного місяця обраного періоду. Результати і висновки. Було розраховано амплітуду зональної асиметрії озону, проаналізовано місячну, широтну, довготну і висотну варіацію. Було показано, що найбільша зональна асиметрія спостерігається навесні, особливо в жовтні, з домінуванням структури

хвилі-1 з зональним мінімумом близько 0°–90° зх.д. і максимумом близько 120°–180° сх.д. Область з високим вмістом озону знаходиться близько 40°–80° пд.ш., і поступово зміщується на південь, з вересня по листопад. Модель занижує амплітуду зональної асиметрії особливо в жовтні. Широтний середній максимум зонально середнього розподілу озону спостерігається близько 62° пд.д. у вересні, 66° пд.д. у жовтні і 68° пд.д. у листопаді для MERRA-2 і близько 64° пд.д., 65° пд.д. і 66° пд.д., відповідно, для CMIP6. Висновки. Зсув до полюсу зональної області з високим вмістом озону триває до березня зі зменшенням вмісту озону, але у квітні змінюється на протилежний — зсув до екватора з підвищенням рівня озону. У вересні зсув знову стає полярним. Для озонової хвилі-1 з місяця в місяць можна спостерігати східне зміщення довготного мінімуму з вересня до жовтня, і на захід, з жовтня по листопад за даними MERRA-2, але за даними CMIP6 зональний мінімум зсувається тільки на схід від вересня до листопада. Максимальна різниця у парціальному тиску озону у висотному розподілі спостерігається в жовтні у стратосфері між висотними максимумами зонального мінімуму і максимуму і становить близько 68% (44%) від значення концентрації озону у зонально середньому висотному максимумі вздовж 65 пд. ш. (65.4 пд.ш.). Вертикальні профілі MERRA-2 на відміну від профілів CMIP6 показують більш високе положення висотного максимуму над зональним мінімумом і нижче — над зональним максимумом з середнім між ними зонально середнім. Всі три вертикальні профілі CMIP6 мають однакове положення висотного максимуму.

Ключові слова: озонова діра, планетарні хвилі, кліматологія, зональна асиметрія, MERRA-2, CMIP6